

A Large Paleolake Basin at the Head of Ma'adim Vallis, Mars

Rossman P. Irwin III,^{1,2*} Ted A. Maxwell,¹ Alan D. Howard,²
Robert A. Craddock,¹ David W. Leverington¹

At 8 to 15 kilometers wide, Ma'adim Vallis is one of the largest valleys in the martian highlands. Although a groundwater source was previously suggested, the channel originates at a spillway in the divide of a ~3,000,000-square-kilometer closed drainage basin. The interior morphology of this source basin, including likely shoreline features following topographic contours, suggests that Ma'adim Vallis was created through catastrophic overflow of a ~1,100,000-square-kilometer highland lake. The size, constant levels, and interior morphology of three regional paleolake basins require a warmer paleoclimate and a long-term, recharged, stable highland water table more than ~3.5 billion years ago.

The exploration of Mars has focused on issues of past or present habitability, and long-lived standing bodies of water may have been the most favorable sites for ancient microbial life (1). During the heavy meteorite bombardment epoch [4.5 to ~3.8 billion years ago (Ga)] (2), large craters frequently disrupted the widespread, contemporaneously active highland valley networks, and the shortened valleys commonly drained to closed drainage basin floors (3). At scattered locations across Mars, these highland craters or intercrater basins may have contained small lakes (1, 4, 5). Evaporation from possible ancient planetary seas in the larger Argyre (6) impact basin and the northern lowlands (7, 8) may have supplied the highland valleys with water, whereas geothermally liberated permafrost is the most widely accepted alternative water source (9).

Regardless of whether Noachian valleys were supplied by precipitation or by an elevated, melting cryosphere, water would collect in the deeper basins. Small, transient crater lakes could have occurred at the termini of some valley networks in an arid environment, but long-lived highland lakes would require an influx of water from stable aquifers, recharged by some combination of precipitation (indicated by dense valley networks heading at sharp divides) and/or regional groundwater. Lacustrine surface morphology also requires long-term standing water, maintained by a warmer paleoclimate. Here we describe a 1,000,000-km² Noachian lake in the southern highlands indicating the location and elevation of an unconfined water

table. This lake drained northward through Ma'adim Vallis, one of the larger martian valleys, with a length of 900 km and a width of 8 to 15 km. The valley's origin has previously been attributed to runoff (10), groundwater sapping (11), or the emergence of voluminous groundwater by chaotic terrain or a fissure (12). We tested these hypotheses for consistency with image data and the topographic grid (1 km/cell) compiled from the Mars Orbiter Laser Altimeter (MOLA) data from the Mars Global Surveyor (MGS) mission (12). These data were not available to earlier investigators of this region, who relied on topography estimated by stereo image pairs (13), atmospheric radio occultation, Earth-based radar, and shadows (14, 15).

MOLA topography reveals that Ma'adim Vallis crosscuts a circular basin, 490 km in diameter, which is probably a highly degraded impact crater (Fig. 1).² The river channel, 3 km wide, originates at a gap in the southern margin of this crater rim (Fig. 2, point B) at 950 m elevation (MOLA datum). Fed by a water supply of >100,000 km³ from the region south of this drainage divide, water flowed northward into the impact basin interior. Before incision ceased, the valley was cut down and headward (southward) to a location ~25 km south of the original ridge crest (Fig. 2, point A). This water gap at the ridge crest is also the lowest possible spill point on the drainage divide of a ~3,000,000-km² closed drainage basin, located to the south of the spillway.

Downstream, the valley was incised more than 500 m into the impact basin floor, and the river exited this basin through a canyon (2100 m deep) cut into the northern rim. On Earth, such water gaps are usually created by ponded water overflowing a drainage divide (16). North of this exit breach, the river debouched to Gusev crater, where ponding supported a ~1500-m valley base level, on the boundary between the elevated highland and

smoother lowland terrains. This crater is also exit breached (17), but Ma'adim Vallis does not continue onto the lowland terrain north of Gusev crater. This is consistent with the behavior of nearly all valley networks crossing the highland-lowland dichotomy (18).

To test for consistency with the overflowing lake hypothesis, we mapped the 950-m contour around the interior of the large closed drainage basin (hereafter informally called the Eridania basin) and examined the surface features on either side of this elevation. A break in slope is commonly located at the 1100-m elevation contour around the Eridania basin interior (Fig. 1A and Fig. 2). Smooth and ridged plains are located below the 1100-m contour, whereas higher-standing terrain is generally steeper and dissected. Mapping of the drainage divides suggests that the 1100-m contour is also about the highest level that a lake could have occupied without spilling over at two other points at 1150 m (a second point on the Ma'adim impact basin ridge and one on the northwestern divide), but no evidence of overflow was observed at these locations. The break in slope also occurs at the 1100-m level in the interiors of breached impact craters that straddle this elevation contour, where the fill slopes downward toward the lake basin interior. These breached craters and the common break in slope may be evidence of shoreline erosion and/or deposition of sediments below a standing water level.

Valley cross sections typically widen where they cross the 1100-m contour, consistent with an abrupt transition from bedrock to less resistant sedimentary materials. The valleys above this level are typically V-shaped and spatially dense, whereas the valleys incised into the plains below 1100 m are considerably wider, commonly with flat floors and undissected interfluves (Fig. 3).³ Around most of the proposed lake shore, valleys do not continue below the 950-m level, despite the presence of appropriate slopes.

The Eridania basin floor has been mapped as a flood volcanic ridged plains unit (19, 20); however, a fluvial sedimentary component in many ridged plains units has since been recognized (3). Although the plains-upland transitional morphology closely follows a contour line, the proposed lake floor is inset with partially ridge-bounded, circular depressions (180 to 270 km in diameter, 0.5 to 1.5 km below the surrounding plains) that are probably degraded impact craters (Fig. 2). If equi-potential volcanic flooding were responsible for the basin-plains boundary at a constant elevation, lavas would have also filled the crater interiors, which is inconsistent with the observed ~1.5 km of vertical relief within the Eridania basin floor.

The bowl-shaped morphology of these depressions is rare among the usually flat-

¹Center for Earth and Planetary Studies, National Air and Space Museum, Smithsonian Institution, Washington, DC 20560, USA. ²Department of Environmental Sciences, University of Virginia, Charlottesville, VA 22904, USA.

*To whom correspondence should be addressed. E-mail: Irwin@nasm.si.edu

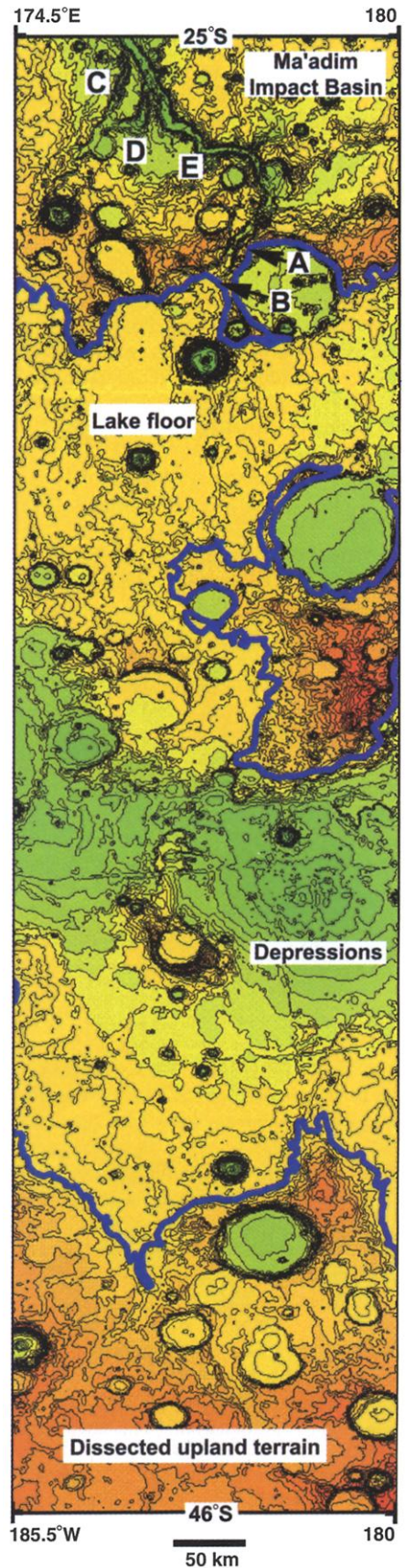
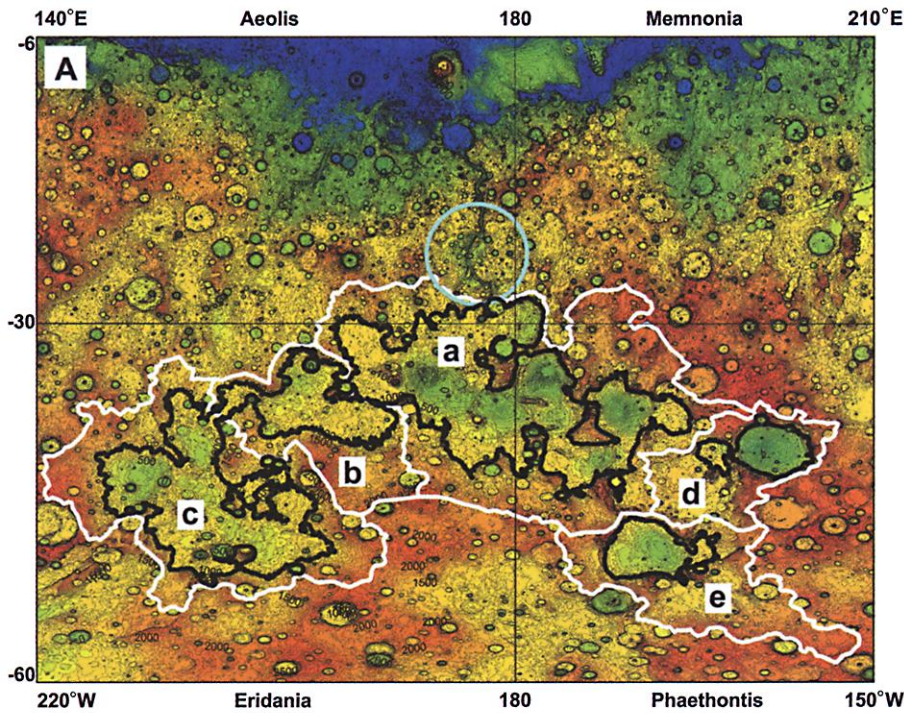


Fig. 1 (left). (A) Topography of lake sub-basins that overflowed to Ma'adim Vallis (a, b, and c) and isolated lake basins (d and e). The blue circle is the Ma'adim impact basin, and drainage divides (white lines) surround the lake's high stand at 1100 m (black line). (B) Topography of Ma'adim Vallis, showing the Ma'adim basin rim crosscut at (c) and at the valley head (a), dissected basin floor (b), Gusev crater (d), its exit breach (e), and undissected lowlands (f). Both figures are MOLA topography (cylindrical projection, 100-m interval).

Fig. 2. (right) MOLA contoured topography (100-m interval, vertical scale as in Fig. 1) at the head of Ma'adim Vallis. The Ma'adim ancient impact basin rim was breached at (A) and cut 25 km southward to (B), which is the drainage divide in the present landscape. Paleocourses developed as the channel cut down and headward into the flat basin floor, with (C) and (D) active first, then the shortest downslope route (E) dominated as incision advanced the channel headward. The plains-upland transition (blue line) and deep lake floor depressions are evident.

REPORTS

floored low-latitude impact craters, which were probably degraded primarily by fluvial processes (21). The unusual shape of these depressions may have resulted from deposition of sediment around the crater margins in standing water, whereas the sediment could have been transported well into the interior in basins affected by a fluvial rather than lacustrine transport regime (22). Along the 180° meridian, these depressions contain the lowest elevations between the South Pole and the northern lowlands, and they would have contained lakes if a stable water table occurred anywhere within 1.5 km of the highland plateau surface. The deepest locations within the larger depressions contain interior mesas or knobby terrain, with a thin, dark, smooth capping layer and rougher, relatively bright flanks. These exhibit recent gullying on several pole-facing slopes (23). This terrain has been jointed and degraded in situ, perhaps as the lake drained and hydraulic support was removed, fracturing the indurated sur-

face layer. With the capping layer removed in places, the less durable materials beneath could be eroded by slope processes and transported by wind (24). The floor of the Eridania lake basin also contains a set of unaligned or circular ridges, suggesting autocompaction of sediment over buried crater and ridge topography rather than tectonic stress, consistent with the lake hypothesis (25).

Fresh crater counts on the Eridania lake basin floor suggest a late Noachian age (26) of >3.5 to 3.7 Ga (2), and the Gusev crater floor deposit has a statistically similar fresh crater density (17) and may be contemporary (Table 1). The longevity of Ma'adim Vallis is also constrained by the incomplete dissection of the valley sidewalls and poor grading of tributaries, which suggest that this valley was active during a relatively short period near the end of the Noachian. If this interpretation is accurate, a relatively large and brief discharge of water created the present valley. Although large discharges from the subsurface (through chaotic terrain or fissures) have been proposed as the source for this and other large martian outflow channels (12, 27), Ma'adim Vallis does not exhibit a chaotic source region or fissure at its head. These features are observed in the region, but 500 km from the valley head and >1 km below it.

These observations suggest the following interpretation for the history of Ma'adim Vallis and its large source basin. A 490-km Noachian impact basin created a drainage divide, isolating a ~3,000,000-km² catchment in the Eridania and Phaethontis quadrangles of Mars. Several superimposed 180- to 270-km craters were responsible for much of this drainage basin's 1.5-km depth. Influenced by the local water table, the Eridania basin filled with water early in its history, allowing time for fluvial valleys on the high-standing terrain and shore erosion to bury much of the lake's interior cratered landscape with sediment. The unusual bowl shape of the deep interior basins suggests that they were filled with water throughout the fluvial epoch, as they never developed the flat floors

typical of most other degraded craters (21). At its greatest extent, the lake occupied an area of ~1,100,000 km² and had a volume of ~480,000 km³, but it did not initially overflow its drainage divide. A <50-m rise in the lake level above the 1100-m contour resulted in the late Noachian outflow into the Ma'adim Vallis impact basin.

The Eridania basin lake would have contained 160,000 km³ of surface water between the 950- and 1100-m contours; however, only 100,000 km³ was available for direct runoff, because ridges isolated parts of the Eridania basin as the lake level declined (Fig. 1A, sub-basins B and C). Incision of the overflow point lowered the lake level, initially filling the Ma'adim impact basin with ~60,000 km³ of stored surface water. Under the influence of the northern lowland base level, the Ma'adim basin probably did not contain a long-lived lake, as its cratered floor is not deeply buried by plains sediments (as the Eridania basin floor is). The Ma'adim basin quickly overflowed and incision began at its northern rim, which also stood at approximately 1000- to 1100-m elevation. At this location the valley cut down and advanced headward, eventually breaching the northern impact basin rim and draining the short-lived Ma'adim lake. Ma'adim Vallis then cut into the Ma'adim basin floor, fed by the 40,000 km³ of remaining surface water above the 950-m contour in the Eridania lake. Another potential 75,000 km³ of slower discharge was available by draining the aquifer and equalizing the levels of then-isolated lakes in the region (Fig. 1A, sub-basins B through E). Throughout this time, Gusev crater acted as a detention pond, slowing the discharge and accumulating 15,100 km³ of sediment (28). Gusev crater was exit breached, and the associated reduction in base level resulted in incision of the downstream inner channel, leaving elevated terraces. As the excavated volume of Ma'adim Vallis is ~14,000 km³, the water/sediment ratio is between 7:1 and 11:1 by volume, depending on potential input by partially draining the aquifer. These are reasonable sediment concentrations for exca-

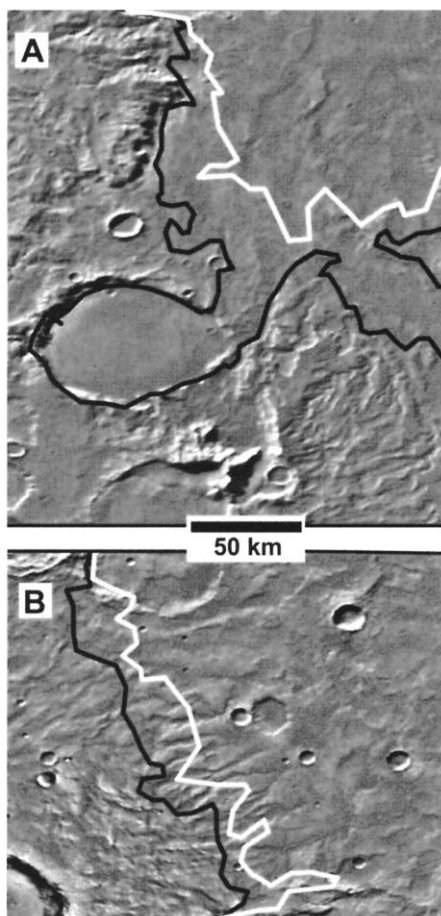


Fig. 3. Shoreline morphology in the lake basin, from Viking 256 pixel/degree mosaics. Valley networks either stop abruptly [(A) centered at 43.75°S, 184.5°E] near the black 1100-m contour, the lake's likely high stand, or widen below that level [(B) centered at 37.5°S, 159°E] if slopes were available in the basin. The white line is the 950-m contour.

Table 1. Impact crater counts for the Eridania basin floor and Gusev crater floor.

Geologic unit	Count (n)	N(2)*	N(5)*	Age [using N(5)]†
Lake floor plains	732	633 ± 27	204 ± 15	Late Noachian near Hesperian boundary (26), >3.5 to 3.7 Ga (2)
Gusev crater floor‡	24	541 ± 221	None	
Ma'adim Vallis‡	5	708 ± 306	None	
Ma'adim delta‡	10	619 ± 206	None	

*N(x) is the number of craters > x km diameter, ± √n error, both normalized to 10⁶ km². †A widespread deficiency of 2-km craters in Noachian units yields incorrect Hesperian ages when N(2) numbers are used. ‡Data are from (17); the large error in their results is due to the small area of Gusev crater and small sample size.

vation by catastrophic floods (29). After this initial flood, possible later flows would have been smaller discharges of Eridania lake sub-basin A (Fig. 1A).

References and Notes

1. N. A. Cabrol, E. A. Grin, *Icarus* **142**, 160 (1999).
2. W. K. Hartmann, G. Neukum, *Space Sci. Rev.* **96**, 165 (2001).
3. R. P. Irwin III, A. D. Howard, *J. Geophys. Res.*, in press.
4. J. A. Grant, *Geology* **28**, 223 (2000).
5. R. D. Forsythe, C. R. Blackwelder, *J. Geophys. Res.* **103**, 31421 (1998).
6. T. J. Parker, S. M. Clifford, W. B. Banerdt, *Lunar Planet. Sci. Conf.* **31**, 2033 (2000).
7. T. J. Parker, R. S. Saunders, D. M. Schneeberger, *Icarus* **82**, 111 (1989).
8. J. W. Head III et al., *Science* **286**, 2134 (1999).

9. D. E. Wilhelms, R. J. Baldwin, *Proc. Lunar Planet. Sci. Conf.* **19**, 355 (1989).
10. R. P. Sharp, M. C. Malin, *Geol. Soc. Am. Bull.* **86**, 593 (1975).
11. N. A. Cabrol, E. A. Grin, R. Landheim, *Icarus* **132**, 362 (1998).
12. N. A. Cabrol, E. A. Grin, G. Dawidowicz, *Icarus* **125**, 455 (1997).
13. D. E. Smith et al., *J. Geophys. Res.* **106**, 23689 (2001).
14. G. D. Thornhill et al., *J. Geophys. Res.* **98**, 23581 (1993).
15. N. A. Cabrol, E. A. Grin, G. Dawidowicz, *Icarus* **123**, 269 (1996).
16. J. E. O'Connor, *Geol. Soc. Am. Spec. Pap.* **274** (1993).
17. N. A. Cabrol, E. A. Grin, R. Landheim, R. O. Kuzmin, R. Greeley, *Icarus* **133**, 98 (1998).
18. M. H. Carr, *Water on Mars* (Oxford Univ. Press, New York, 1996).
19. D. H. Scott, K. L. Tanaka, *U.S. Geol. Surv. Misc. Invest. Ser. Map I-1802-A* (1986).

20. R. Greeley, J. E. Guest, *U.S. Geol. Surv. Misc. Invest. Ser. Map I-1802-B* (1987).
21. R. A. Craddock, T. A. Maxwell, A. D. Howard, *J. Geophys. Res.* **102**, 13321 (1997).
22. A. D. Howard, *Eos* **81** (fall meet. suppl.), abstract P62C-06 (2000).
23. M. C. Malin, K. S. Edgett, *Science* **288**, 2330 (2000).
24. L. S. Manent, F. El-Baz, *Earth Moon Planets* **34**, 149 (1986).
25. H. V. Frey, K. M. Shockey, J. H. Roark, E. L. Frey, S. E. H. Sakimoto, 2001 GSA Annual Meeting, Boston, MA, 5 to 8 November 2001 (abstract 25358).
26. K. L. Tanaka, *J. Geophys. Res.* **91**, E139 (1986).
27. M. H. Carr, *J. Geophys. Res.* **84**, 2995 (1979).
28. P. D. Komar, *Icarus* **42**, 317 (1980).
29. B. L. Carter, H. Frey, S. E. H. Sakimoto, J. Roark, *Lunar Planet. Sci. Conf.* **32**, 2042 (2001).
30. Supported by NASA grants NAG5-3932 and NAG5-9817.

2 February 2002; accepted 3 May 2002

The Mass Disruption of Oort Cloud Comets

Harold F. Levison,^{1*} Alessandro Morbidelli,² Luke Dones,¹ Robert Jedicke,³ Paul A. Wiegert,⁴ William F. Bottke Jr.¹

We have calculated the number of dormant, nearly isotropic Oort cloud comets in the solar system by (i) combining orbital distribution models with statistical models of dormant comet discoveries by well-defined surveys and (ii) comparing the model results to observations of a population of dormant comets. Dynamical models that assume that comets are not destroyed predict that we should have discovered ~100 times more dormant nearly isotropic comets than are actually seen. Thus, as comets evolve inward from the Oort cloud, the majority of them must physically disrupt.

It has been over half a century since Jan Oort first argued that a roughly spherical cloud of comets, which extends to heliocentric distances larger than 100,000 astronomical units (AU), surrounds the solar system (1). This structure, which is now known as the Oort cloud, is currently feeding comets into the inner solar system (with perihelion distances, q , of less than 3 AU) at a rate of about 12 comets per year with an active comet absolute magnitude, H_{10} , <10.9 (2, 3). These comets as a whole are known as nearly isotropic comets (NICs) (4). NICs can be divided into the following two subpopulations, based on their dynamical histories (5): (i) dynamically new NICs, which are on their first pass through the system and typically have semi-major axes, a , greater than ~10,000 AU, and (ii) returning NICs, which have previously passed through the inner solar system and typically have $a \leq 10,000$ AU.

One unsolved problem is that models of the orbital evolution of new NICs into returning NICs consistently predict many times more returning comets than are observed (2, 6). This so-called "fading problem" cannot be due to previously unmodeled dynamical effects (2) and thus must be due to the physical evolution of the comets' activity (7). An important issue, therefore, is to determine the fate of the missing comets; either they become extinct or dormant (8), or they disintegrate entirely (9, 10). Here, we try to distinguish between these two possible outcomes by comparing model results to observations of dormant comets.

Large ground-based surveys have discovered 11 asteroidal objects, as of 3 December 2001, that are on orbits consistent with active NICs with $q < 3$ AU (Table 1) (11) [see supporting online material (SOM)]. These 11 objects represent just a small fraction of the total population of dormant NICs, because ground-based surveys suffer from unavoidable observational biases (12). Thus, the main purpose of the work presented here is to estimate the total number of dormant NICs based on the available data. We accomplish this by the following steps: (i) we use numerical simulations of cometary dynamics to produce a

set of fictitious dormant NICs, (ii) we run these fictitious NICs through a near-Earth object (NEO) survey simulator to determine which ones would be discovered, and (iii) we compare the results of (ii) to observations of the known dormant NICs to estimate the total number and orbital element distribution of the entire real dormant NIC population.

We determined the expected orbital element distribution for the dormant NICs from long-term dynamical simulations that track thousands of fictitious new comets entering the planetary system from the Oort cloud for the first time. The simulations calculate the dynamical evolution of these objects' orbits caused by the gravitational influence of the Sun, planets, and Milky Way Galaxy. The objects' trajectories are followed until they are either ejected from the solar system, hit a planet, or strike the Sun. From this, we can develop a steady-state distribution of NICs by assuming that the influx rate of dynamically new comets is constant with time.

We used simulations that were performed elsewhere (2, 13). Because of differing computational challenges, these simulations have

Table 1. Known dormant NICs.

Asteroid Desig.	a (AU)	e	i (Deg)	q (AU)	H
(15504)1999 RG ₃₃	9.4	0.77	35	2.1	12.1
2000 DG ₈	10.8	0.79	129	2.2	12.8
(5335) Damocles	11.8	0.87	62	1.6	13.3
2001 OG ₁₀₈	13.3	0.93	80	1.0	13.0
1998 WU ₂₄	15.2	0.91	43	1.4	15.0
1999 XS ₃₅	18.0	0.95	19	0.95	17.2
(20461)1999 LD ₃₁	24.0	0.90	160	2.4	13.8
2000 HE ₄₆	24.0	0.90	158	2.4	14.6
1997 MD ₁₀	26.7	0.94	59	1.5	16.0
2000 AB ₂₂₉ *	52.5	0.96	69	2.3	14.0
1996 PW*	287	0.99	30	2.5	14.0

The columns are: Desig., designation; a , semi-major axis; e , eccentricity; i , inclination; q , perihelion distance; and H , Absolute Magnitude. See text for definitions. *All are type HTC, except the last two, which are ERCs.

¹Southwest Research Institute, 1050 Walnut Street, Suite 426, Boulder, CO 80302, USA. ²Observatoire de la Cote d'Azur, B. P. 4229, 06034 Nice Cedex 4, France. ³Lunar and Planetary Laboratory, University of Arizona, Tucson, AZ 85721, USA. ⁴Department of Physics, Queen's University, Kingston, Ontario K7L 3N6, Canada.

*To whom correspondence should be sent. E-mail: hal@gort.boulder.swri.edu